Aggregation Phenomena of Model PS/PI Super-H-Shaped Block Copolymers. Influence of the Architecture

Hermis Iatrou,[†,‡] Lutz Willner,[*,§] Nikos Hadjichristidis,[‡] Avi Halperin,[||] and Dieter Richter[§]

Department of Chemistry, The University of Athens, 15771 Athens, Greece, Institut für Festkörperforschung, Forschungszentrum Jülich GmbH, D-52425 Jülich, Germany, and CRPCSS, 24 av President Kennedy, 68200 Mulhouse, France

Received June 26, 1995; Revised Manuscript Received October 25, 1995[⊗]

ABSTRACT: The super-H-shaped block copolymers belong to a new class of polymeric materials, the miktoarm stars (mikto from the Greek word μικτος meaning mixed), which includes star-shaped polymers in which from one or more junction points radiate different arms. Schematically, the super-H structure can be described as two three-arm stars which are bridged with a common fourth arm. Model super-H-shaped block copolymers of the PI_3(PS-d_8)PI_3 type, where PI is protonated polyisoprene and PS-d_8 is deuterated polystyrene, were synthesized by anionic polymerization using the chlorosilane approach. These nonlinear block copolymers were characterized by size exclusion chromatography (SEC), ultraviolet (UV) spectroscopy, low-angle laser light scattering (LALLS), and membrane (MO) and vapor pressure osmometry (VPO). The micellar behavior of these stars was investigated in *n*-decane, which is a selective solvent for the PI part. Small angle neutron scattering (SANS), LALLS, and viscometry were used in order to characterize the micelles. SANS measurements were performed at two different contrasts, where in each case one of the monomeric units was matched to the solvent. The coherent scattering cross sections of the single cores and coronas were determined by extrapolating low-concentration data to $\phi = 0$. A theoretically calculated cross section of an unswollen hard sphere of PS-d_8 was found to fit fairly well the experimental curves for the core. A calculated cross section of a hollow sphere with a constant density profile for the PI chains was found to describe the cross sections of the corona. Experimentally, it was found that the super-H structure increases the solubility and drastically reduces the aggregation number in comparison with linear PS/PI diblocks. A scaling approach is presented to take into account the specific influence of the SH structure on the micellar properties. It was found that the derived scaling laws of an intermediate regime between the starlike and the crewcut regime are in fair agreement with the experimental observations.

1. Introduction

In the past 20 years, the behavior of amphiphilic block copolymers at interfaces has been a subject of great interest. The diblock copolymers in a selective solvent present similarities with surfactants. This allows studies of properties such as detergency, surfactancy, colloidal dispersion, and stabilization. Many groups have studied the micellar[4] behavior of block copolymers in a selective solvent for one of the blocks with a variety of techniques, such as low-angle and dynamic laser light scattering,[5−8] viscometry,[9,10] SANS,[11] and small angle X-ray scattering (SAXS).[12,13] Moreover, some review papers have been presented.[1−3]

However, only a limited amount of studies present systematic investigation of the influence of the molecular characteristics of the polymers to the micellar properties.[5,6,37] Moreover, almost all research is restricted to linear diblock or triblock copolymers of the AB or ABA type, respectively.

The availability of model polymers with new well-defined structure and low degrees of molecular and compositional heterogeneity can facilitate the further understanding of the polymer structure−property relationship.

Recently, the synthesis of miktoarm star copolymers has received much attention. It has been shown that the segregated bulk morphology of the miktoarm star copolymers is different from that of a linear diblock or triblock copolymer of the same composition.[14]

In the present paper we will examine the micellar behavior of the super-H-shaped (*SH*) block copolymers of the PI_3(PS-d_8)PI_3 type (see Scheme 1). Six SH-shaped block copolymers with a PS fraction from 8 to 60 w % have been synthesized and characterized by size exclusion chromatography, UV spectroscopy, membrane and vapor pressure osmometry, laser differential refractometry, and low-angle laser light scattering.

SANS, LALLS, and viscometry were used to examine the structural properties of the micelles formed in *n*-decane. *n*-Decane is a nonsolvent for PS-d_8 and assumed to be a good solvent for PI. The SANS measurements were performed either in core or in shell contrast such that the structural information of both parts could be determined separately. Using the results of the three methods, it became possible to determine the weight average molecular weight of the micelles, M_W(M), the radius of the cores, R_c, the thickness of the coronas, H, and the aggregation numbers, p_W. We observed that the super-H block copolymers with a small fraction of PS-d_8 do not aggregate under the experimental conditions. Those with an increased fraction of polystyrene form near monodisperse spherical micelles. The aggregation numbers of these micelles are considerably lower than those formed by linear PS/PI block copolymers.[6]

We will discuss the experimental observations in terms of scaling ideas. The discussion is based on the *starlike*[38] and *intermediate*[40] micellar structure allowing for the number of PI branches. It is shown that the experimental results of both super-H and linear PS/PI

* To whom correspondence should be addressed.
† Presently at the Institut für Festkörperforschung.
‡ University of Athens.
§ Institut für Festkörperforschung.
|| CRPCSS.
⊗ Abstract published in *Advance ACS Abstracts,* December 15, 1995.

0024-9297/96/2229-0581$12.00/0

Scheme 1

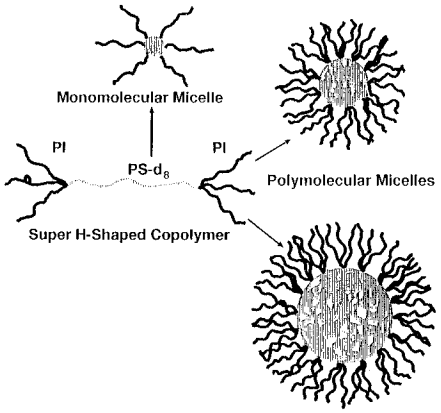

block copolymers are in agreement with the predictions of the *intermediate* model. These arguments also explain qualitatively the higher cmc in this system.

2. Experimental Section

2.1. Synthesis and Characterization of the Copolymers and Micelles. The purification procedures for monomers, linking agents, and solvents to the standards required for anionic polymerization have been described in detail elsewhere.[15,16] *sec*-Butyllithium, prepared in vacuo from *sec*-butyl chloride and a lithium dispersion, was used as initiator for the preparation of the PI arms. The connector, i.e. the polymer that will constitute the central bridge of the six arms was prepared separately with sodium naphthalenide as the initiator.[16] All manipulations were performed in evacuated, *n*-BuLi-washed, and benzene-rinsed glass reactors provided with breakseals and constrictions.[17] The purification of St-d_8 was performed in the same way as for the protonated monomer.

The basic reactions used for the synthesis of the super-H-shaped copolymers of the $PI_3(PS\text{-}d_8)PI_3$ type are schematically the following:

$$\text{naphthalene} + \text{Na} \rightarrow \text{sodium naphthalenide} \qquad \text{(I)}$$

$$\text{St-}d_8 + \text{I} \rightarrow \text{Na(PS-}d_8\text{)Na} \qquad \text{(II)}$$

$$\text{II} + \text{excess } SiCl_4 \rightarrow Cl_3Si(PS\text{-}d_8)SiCl_3 + 2NaCl + SiCl_4\uparrow \qquad \text{(III)}$$

$$\text{III} + \text{excess PILi} \rightarrow \underset{\text{SH-shaped copolymer}}{(PI)_3(PS\text{-}d_8)(PI)_3} + 6LiCl + PI$$

where St-d_8 is deuterated styrene monomer. The copolymers will be identified by the molecular weights of the PS-d_8 connector and PI arm, respectively; e.g. SH 80−10 means that the connector has a molecular weight of about 8×10^4 and the arm 1×10^4.

The preparation of the initiator and of the difunctional PS-d_8 connector has already been described in previous papers.[24,25] The linking reaction of the living difunctional connector with the tetrachlorosilane was performed in a similar way described by Iatrou and Hadjichristidis.[17,18] A small aliquot (∼1 g) of the PI arms and the connector was always removed for characterization. In the case of the SH 40−10, 80−10, and 10−10, a large amount of PI living chains were prepared and split in three parts. Therefore, the molecular weights of the PI arms were identical. The synthetic procedure was monitored via SEC.

In all cases the SEC chromatogram of the hexafunctional macromolecular linking agent (III) was almost indistinguishable from the parent material (II). A typical example is given in Figure 1. The raw product and the fractionated SH copolymer are shown in Figure 2. In some cases the raw product appeared with two additional peaks (see Figure 3). The traces of the high molecular weight polymer that appears after the linking reaction is due to the coupled material PI_3-$Si(PS\text{-}d_8)(PI)Si(PI)(PS\text{-}d_8)SiPI_3$. The polymer that appears between the excess of the PI arm and the SH copolymer is due either to the reaction of a monofunctional connector with $SiCl_4$ or to insufficient elimination of the excess of the linking agent. In the former case this side product is the corresponding $(PS\text{-}d_8)(PI)_3$ four-miktoarm star copolymer and in the latter case the $(PI)_4$ four-arm symmetric homostar. By increasing the excess of the silane, decreasing the temperature of the linking reaction, and taking care of all the above experimental parameters, it was possible to reduce the side products to less than 5%.

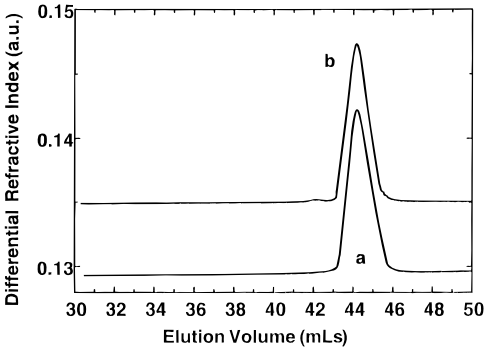

Figure 1. SEC chromatograms of the PS-d_8 connector (a) and the α,ω-bis(trichlorosilane)-capped PS-d_8 (b) of copolymer SH 20−20.

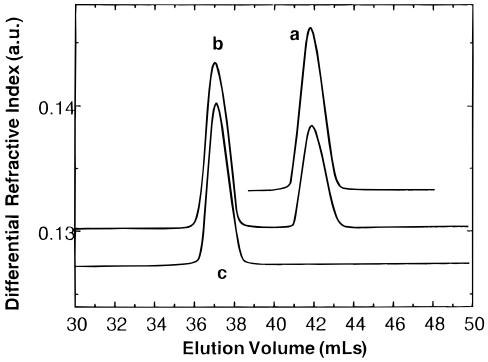

Figure 2. SEC chromatograms of the PI arm (a) and of the unfractionated (b) and fractionated copolymer SH 20−20 (c).

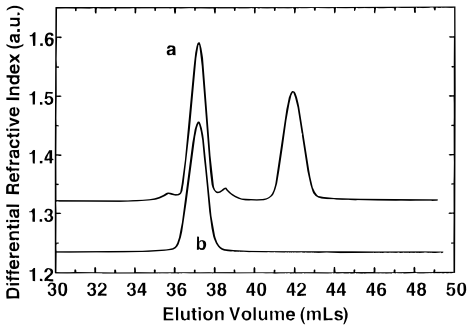

Figure 3. SEC chromatograms of the unfractionated (a) and fractionated (b) copolymer SH 40−20.

Fractionation of the super-H-shaped copolymers was performed by addition of methanol to a 0.1−0.5% solution of toluene. After the fractionation, all the side products were eliminated, and the SEC chromatograms showed higher than 99% purity for the SH-shaped copolymers.

SEC experiments were carried out at 25 °C using a Waters 150C instrument. Four μ-Styragel columns with a continuous porosity range from 10^5 to 500 Å were used together with one ultra-Styragel column of continuous porosity. Tetrahydrofuran (THF) was the carrier solvent at a flow rate of 1 mL/min. SEC experiments were also performed with a refractive index and UV detector in series for the analysis of the polymer composition over the elution peak.

The weight-average molecular weight M_W(SH) of the SH stars and the micelles M_W(M) was measured with a Chromatix

Table 1. Molecular Characteristics of PS/PI Super-H-Shaped Block Copolymers

sample	M_N[a] × 10^{-4} PS-d_8	M_N[a] × 10^{-4} PI	M_N[a] × 10^{-4} SH	A_2[a] × 10^4 (mL mol g^{-2})	M_W(SH)[b] × 10^{-4}	A_2[b] × 10^4 (mL mol g^{-2})	M_W/M_N[c]	dn/dc[e]	amt of PS-d_8 (w %) M_N[f]	amt of PS-d_8 (w %) UV
SH 10−20	0.84[d]	1.56	10.8	8.1	10.9	7.8	1.04	0.140	8.2	8.5
SH 10−10	0.84[d]	1.03[d]	6.87	9.1	7.13	7.6	1.04	0.143	11.5	12
SH 20−20	1.68	1.79	12.0	10.0	12.8	7.5	1.03	0.144	13.5	14
SH 40−20	4.59	1.56	14.1	7.5	14.9	6.8	1.03	0.148	33	33
SH 40−10	4.59	1.03[d]	10.6	7.0	11.4	6.3	1.04	0.157	43	42
SH 80−10	8.46	1.03[d]	15.1	6.5	15.4	5.9	1.03	0.165	58	57

[a] Membrane osmometry in toluene at 37 °C. [b] LALLS in THF at 25 °C. [c] SEC in THF at 25 °C. [d] VPO in toluene at 50 °C. [e] Laser differential refractometry in THF at 25 °C. [f] Calculated from M_N of connector and arms.

KMX-6 low-angle laser photometer. This instrument is equipped with a helium−neon laser and operates at a wavelength of 633 nm. THF and *n*-decane, purified over sodium and distilled prior to use, were the solvents at 25 °C. The refractive index increments dn/dc in THF or *n*-decane at 25 °C were measured with a Chromatix KMX-16 refractometer operating at 633 nm and calibrated with aqueous NaCl solutions. In all cases the M_W values were obtained from $(Kc/\Delta R_\theta)^{1/2}$ vs c plots (ΔR_θ, excess Rayleigh ratio; K, combination of known optical and instrument constants; c, concentration) in order to minimize the curvature due to the third virial coefficient. In all cases the correlation coefficient was better than 0.99.

The number-average molecular weights (M_N) were determined with a Wescan Model 230 membrane osometer (MO) at 37 °C and in a few cases ($M_N < 1.3 \times 10^4$) with a Wescan Model 233 vapor pressure osmometer (VPO) at 50 °C. Toluene, distilled over CaH_2, was the solvent. The M_N values from MO were obtained from $(\pi/c)^{1/2}$ vs c plots, where π is the osmotic pressure. In the case of VPO, the M_N values were obtained from the $(\Delta R/c)$ vs c plots (ΔR is the change in the resistance of the thermistors) using the relation $(\Delta R/c)_{c\to 0} = k_v/M_N$, where k_v is the calibration constant. In all cases the correlation coefficient was better than 0.99.

The PI arms were analyzed by ^{13}C and ^1H NMR spectroscopy in $CDCl_3$ at 25 °C and were found to have the following typical microstructures: 10 w%, 3,4, 70 w % cis 1,4 and 20 w % trans 1,4. The composition of the super-H-shaped copolymers was obtained from the UV−SEC chromatograms.

In order to examine the micellar behavior, two series of copolymers were prepared, one with low PS-d_8 content, i.e. SH 10−10, SH 10−20, and SH 20−20, and another with higher PS-d_8 content, i.e. SH 40−20, SH 40−10, and SH 80−10. The characteristics of the precursors and the fractionated SH star copolymers are given in Table 1.

The narrow molecular weight distribution, $M_W/M_N \leq 1.04$ and the good agreement between the values found by osmometry and the calculated one from $M_N(SH) = M_N(con) + 6M_N(arm)$ indicate the high degree of homogeneity in molecular weight and composition of the super-H-shaped copolymers prepared. This fact is also supported by the good agreement between the apparent molecular weight obtained by LALLS and the M_W calculated from the M_N(SH) multiplied with the polydispersity index. There is also good agreement between the PS content of the SH copolymers calculated from the M_N of the connector and the arms and that found by UV results.

Intrinsic viscosities have been measured in *n*-decane at 25 °C. Cannon−Ubbelohde viscometers with a Schott-Geräte automatic timer were used. Solvent flow times (t_0) were typically 150 s. For that type of viscometer the flow times were sufficient, and no corrections were needed. Measurements were performed on four or five concentrations obtained by dilution in the viscometer. The intrinsic viscosities $[\eta]$ were determined from η_{sp}/c and $(\ln \eta_r)/c$ against c plots, where η_{sp} and η_r are the specific and relative viscosities, respectively.

2.2. Small Angle Neutron Scattering Experiments. In general, the scattering cross section dΣ/(Q)dΩ of a PS/PI block copolymer can be expressed as the sum of the partial scattering functions:[19]

$$\frac{d\Sigma}{d\Omega}(Q) = \frac{1}{N_L}[\Delta\rho_{PI}{}^2 I(Q)_{PI} + \Delta\rho_{PS}{}^2 I(Q)_{PS} + 2\Delta\rho_{PI}\Delta\rho_{PS} I(Q)_{PIPS}] \quad (1)$$

Here Q is the scattering vector given by $4\pi \sin(\theta/2)/\lambda$, where θ is the scattering angle and λ is the neutron wavelength. N_L denotes the Avogadro constant and $I(Q)_P$ the static scattering function of the P polymeric component. $\Delta\rho_P{}^2$ is defined as the contrast factor between the polymer P and the solvent:[21]

$$\Delta\rho_P{}^2 = \left(\frac{\Sigma b_P}{v_P} - \frac{\Sigma b_S}{v_S}\right)^2 \quad (2)$$

Σb_S and Σb_P are the coherent scattering lengths, and v_S and v_P, the volumes of the solvent molecule and the repeat units, respectively.

According to eq 1, when we match the PI part by an isotopic solvent mixture, then $\Delta\rho_{PI} = 0$ and eq 1 is transformed to

$$\frac{d\Sigma}{d\Omega}(Q) = \frac{1}{N_L}[\Delta\rho_{PS}{}^2 I(Q)_{PS}] \quad (3)$$

This situation will be referred to as core contrast in the following. When we match the PS-d_8, then $\Delta\rho_{PS} = 0$, and eq 1 is transformed to the following:

$$\frac{d\Sigma}{d\Omega}(Q) = \frac{1}{N_L}[\Delta\rho_{PI}{}^2 I(Q)_{PI}] \quad (4)$$

Accordingly, this condition will be called shell contrast.

The static scattering function can be also expressed as the product of the form factor, $P(Q)$, and the intermolecular structure factor $S(Q)$:

$$I(Q) = \phi V_W P(Q) S(Q) \quad (5)$$

For infinite dilutions $S(Q)$ equals unity and contributions from interparticle interactions are removed.

In order to determine the molecular characteristics we have used the Berry approach:[33]

$$\sqrt{\frac{\phi}{I(Q)}} = \left[\frac{1}{V_W} + \frac{Q^2 R_G{}^2}{3V_W} + 2A_2\phi\right]^{1/2} \quad (6)$$

where V_W is the weight average molecular volume, R_G is the radius of gyration, and A_2 is the second virial coefficient.

The SANS measurements were performed on the PAXE instrument at the Laboratoire Léon Brillouin in Saclay, France. The copolymers were measured either in core or in shell contrast by using solvent mixtures of deuterated and protonated *n*-decane. This was possible, since the coherent scattering length density of protonated *n*-decane ($\Sigma b_D/v = -4.89 \times 10^9$ cm^{-2}) is lower and of deuterated *n*-decane ($\Sigma b_{D-d_{22}}/v = 6.58 \times 10^{10}$ cm^{-2}) is higher than those of PI ($\Sigma b_{PI}/v = 2.68 \times 10^9$ cm^{-2}) and PS-d_8($\Sigma b_{PS-d_8}/v = 6.36 \times 10^{10}$ cm^{-2}), respectively. The volume fraction x of the deuterated solvent species was calculated according to the simple additivity rule:[22,23]

$$\rho_m = x\rho_D + (1 - x)\rho_H \quad (7)$$

Thus, core contrast is obtained with $x = 0.11$ and shell contrast with $x = 0.97$ of deuterated decane.

Three different concentrations were measured for each copolymer in each contrast, approximately 0.5, 1, and 2% v/v. In the case of samples with shell contrast, 2 mm quartz cells

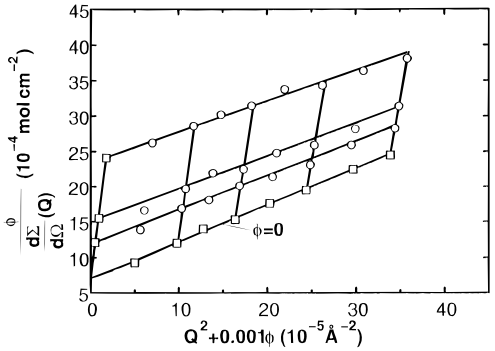

Figure 4. Concentration dependent Zimm plot of copolymer SH 20−20. Measurements under shell contrast. Concentrations: ϕ = 0.5, 1, and 2%.

were used. Transmissions were between 75 and 83%. Solutions under core contrast with mainly protonated solvent were measured in 1 mm quartz cells. With this combination, the transmissions of the solutions were between 0.45 and 0.55.

All SANS experiments were performed at room temperature using two different spectrometer setups. For the small Q range a sample to detector distance of 5 m and a wavelength of 8.8 Å was used. For high Q a distance of 1.8 m and a neutron wavelength of 5 Å was chosen. Thus, a range of the scattering vector of 0.004 Å^{-1} ≤ Q ≤ 0.15 Å^{-1} was covered. The wavelength spread was $\Delta\lambda/\lambda$ = 12%. The raw data were corrected for background, empty cell, and solvent. Detector sensitivity corrections and transformation to absolute scattering cross sections were made with a water standard:

$$\frac{d\Sigma}{d\Omega}(Q) = \frac{I_S(Q)}{I_W(Q)} \frac{MON_W}{MON_S} \frac{d_W}{d_S} \frac{T_W}{T_S} \left(\frac{d\Sigma}{d\Omega}\right)_W \qquad (8)$$

where W refers to the water standard and S to the sample. MON denotes the total monitor counts, d the cell thickness, and T the transmission. $I_S(Q)$ is the scattered intensity of the sample, and $I_W(Q)$ is the scattered intensity of the water standard. $(d\Sigma/d\Omega)_W$ = 0.738 cm^{-1} for water at 5 Å and 0.901 cm^{-1} at 8.8 Å. Finally, incoherent scattering contributions caused by the protonated polymer were calculated and subtracted.

The solutions of micelles were prepared by dilution of a 2% stock solution. It was found that it was necessary to heat the solutions at 70 °C for 1 h in order to dissolve the super-H-shaped copolymers with higher PS-d_8 content. After the dilutions, all the solutions were heated again.

3. Results

3.1. SANS Measurements. Coherent scattering cross sections, $d\Sigma/d\Omega$, of the samples were obtained according to the procedures outlined in section 2. After normalization with the concentration the scattering cross sections fall on top of each other in the intermediate and high Q ranges. Small deviations were found at low Q due to structure factor contributions.

In the case of the shell contrast the $S(Q)$ contributions were removed by extrapolation to infinite dilution. For this purpose we have used concentration dependent Zimm plots as already applied for the determination of star form factors.[34] A typical plot is shown in Figure 4. The obtained scattering cross sections of the single micelles, $d\Sigma(Q, \phi \rightarrow 0)/d\Omega$, of SH copolymers 80−10, 40−20, and 40−10 are shown in Figures 5−7. The scattering curves exhibit well-developed structures with maxima up to the third order. Apparently, aggregates are formed by these copolymers containing an increased polystyrene part. The sharpness of the peaks implies a low polydispersity of these aggregates and a well-separated corona.

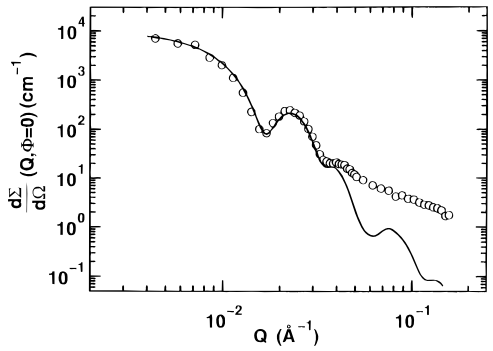

Figure 5. Scattering cross section $d\Sigma(Q,\phi\rightarrow0)/d\Omega$ under shell contrast for copolymer SH 80−10. The solid line represents the calculated cross section of a hollow sphere.

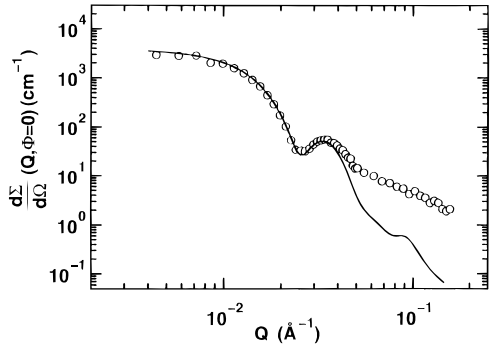

Figure 6. Scattering cross section $d\Sigma(Q,\phi\rightarrow0)/d\Omega$ under shell contrast for copolymer SH 40−10. The solid line represents the calculated cross section of a hollow sphere.

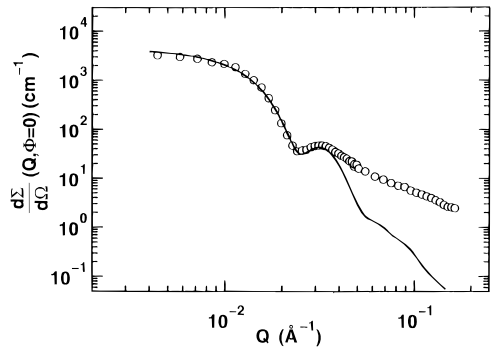

Figure 7. Scattering cross section $d\Sigma(Q,\phi\rightarrow0)/d\Omega$ under shell contrast for copolymer SH 40−20. The solid line represents the calculated cross section of a hollow sphere.

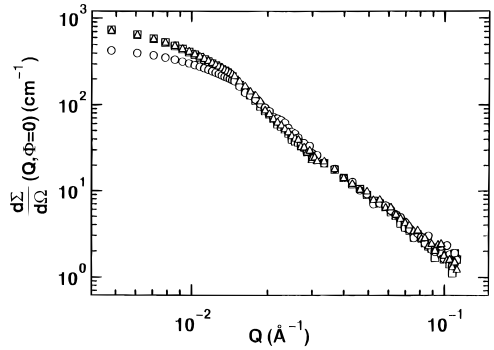

Figure 8. Scattering cross sections $d\Sigma(Q,\phi\rightarrow0)/d\Omega$ under shell contrast of the nonaggregated copolymers: SH 10−10 (○); SH 20−20 (□); SH 10−20 (△).

Shell contrast measurements for SH copolymers 20−10, 10−10, and 10−20 with a relatively small PS-d_8 part are shown in Figure 8. From this plot it becomes obvious that these block copolymers do not form aggregates under the experimental conditions since there

Table 2. SANS−MO Results for Copolymers SH 10−20, 10−10, and 20−20

sample	total molecular weight of PI arms × 10^{-4}		R_G SANS (Å)		R_G	$A_2 \times 10^4$	ν
	SANS (Berry)	MO: M_N(arm) × 6	Berry plots	Benoit approx	(6-arm PI star) (Å)	(mL mol g^{-2})	
SH 10−20	9.36	9.0	102	114	85	5.0	0.54
SH 10−10	6.18	6.3	86	97	66	4.1	0.54
SH 20−20	10.7	9.9	108	118	93	4.0	0.55

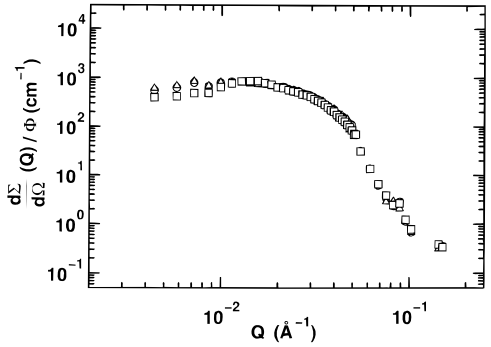

Figure 9. Concentration-normalized scattering cross sections dΣ(Q)/dΩ under core contrast for copolymer SH 40−20 for different concentrations: ϕ = 2% (□); 1% (○); 0.5% (△).

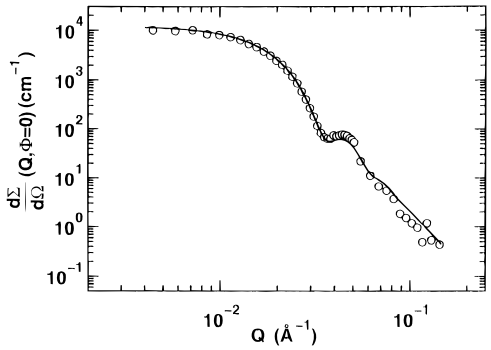

Figure 10. Scattering cross section dΣ(Q,ϕ→0)/dΩ under core contrast for copolymer SH 80−10. The solid line represents the calculated cross section of a sphere.

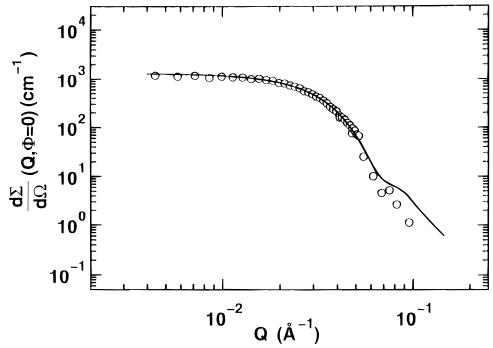

Figure 11. Scattering cross section dΣ(Q,ϕ→0)/dΩ under core contrast for copolymer SH 40−10. The solid line represents the calculated cross section of a sphere.

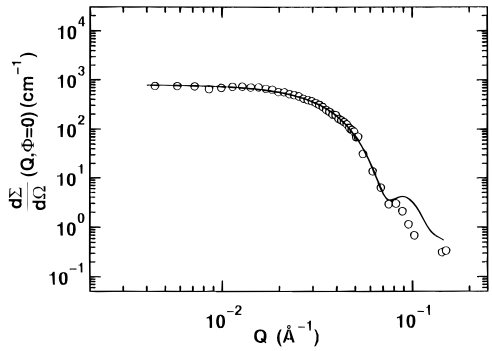

Figure 12. Scattering cross section dΣ(Q,ϕ→0)/dΩ under core contrast for copolymer SH 40−20. The solid line represents the calculated cross section of a sphere.

is no sign of structure. In order to verify this conjecture we have determined the molecular weights using concentration dependent Berry plots according to eq 6. In case there is no aggregation the molecular weight of the PI part, M_W(PI), should correspond to 6 × M_N(arm) measured by membrane osmometry. Both values are listed in Table 2 together with radii of gyration and A_2 values. By comparison it is evident that no aggregates are formed by these copolymers.

Under core contrast conditions, the scattering cross sections of the aggregating copolymers 80−10, 40−10, and 40−20 reveal the development of a shallow correlation peak at low Q at the higher concentrations measured. The structure factor was more pronounced here because it appears at the plateau of the curve. Figure 9 shows the scattering curves of SH copolymer 40−20 for the different concentrations. Because of the peak influence, a complete removal of $S(Q)$ contributions could not be performed by using a concentration dependent Zimm plot. As a first approximation to dΣ(Q,ϕ→0)/dΩ, Q values smaller than 0.012 Å were extrapolated to zero concentration and then added to dΣ/dΩ of the lowest concentration. However, an accurate determination of molecular weights and radii of gyration of the PS core was not possible since the structure factor peak causes a strong curvature in the Guinier range. Scattering cross sections, dΣ(Q,ϕ→0)/dΩ are shown in Figures 10−12. It can be seen that analogous to the shell contrast measurements the curves exhibit a well-pronounced structure.

It should be mentioned here that the corresponding measurements of the nonaggregating copolymers show very poor statistics. This is due to the very small effective concentration of the PS-d_8 part and the high incoherent background of the protonated solvent. Therefore, the data were not further evaluated.

In order to determine the radii of the core and of the shell, theoretical scattering cross sections of a homogeneous sphere and of a hollow sphere, respectively, were fitted to the experimental data. The theoretical curve for the core was calculated by

$$\frac{d\Sigma}{d\Omega}(Q) = 12\pi\phi_{PS-d_8}\frac{\Delta\rho^2(\sin(V_c) - V_c\cos(V_c))^2}{Q^3 V_c^3} \quad (9)$$

where ϕ_{PS-d_8} is the volume fraction of the deuterated polystyrene and $V_c = QR_c$, with R_c the radius of the core.

A corresponding equation was used for the calculation of the shell:

$$\frac{d\Sigma}{d\Omega}(Q) = 12\pi\phi_{PI}\frac{\Delta\rho^2[(\sin(V_0) - V_0\cos(V_0)) - (\sin(V_c) - V_c\cos(V_c))]^2}{Q^3(V_0^3 - V_c^3)} \quad (10)$$

Here ϕ_{PI} denotes the volume fraction of the polyisoprene part and $V_0 = QR_0$ with R_0 as the overall radius of the micelle.

Table 3. Fit Parameters for Copolymers SH 40−10, 40−20, and 80−10

	core parameters				shell parameters		
sample	R_c (Å)	$\Delta\rho^2$ [b] $\times 10^{-21}$ (cm^{-4})	smearing σ(Å)	ν[a]	R_o (Å)	$\Delta\rho^2$ [b] $\times 10^{-21}$ (cm^{-4})	smearing σ(Å)
SH 40−20	63	3.3		0.61	180	1.50	16
SH 40−10	69	3.2		0.67	170	1.48	12
SH 80−10	130	3.4	5	0.68	245	1.51	5

[a] Determined by a power law fit in the asymptotic high Q range. [b] The calculated value is 3.7×10^{21} cm^{-4}.

In order to obtain a good agreement with the experimental curves the calculated scattering cross sections were convoluted by a Gaussian type resolution function taking into account experimental parameters like wavelength spread, finite collimation, and detector resolution according to Pedersen et al.[26] Furthermore, the sharp edge of the polymer density distribution at the boundary of the sphere was smeared by multiplication with a Gaussian in Q space. For the hollow sphere such a smearing was applied only to the overall radius.

During the calculation for the core, $\Delta\rho^2$, R_c, and the smearing range, σ_c, were adjustable parameters. Thus, a good agreement was obtained, as can be seen from Figures 10−12. The corresponding parameters are listed in Table 3. For copolymers SH 40−10 and 40−20 the secondary peaks which appear at relatively high Q values are not clearly developed, due to the limited number of data points in this range. Therefore, the smearing is not very sensitive to the result of the fits and, consequently, we omitted these numbers in Table 3. Small deviations in the intensity were found at high Q values. These are due to the low accuracy of the measured curves in this range. Since we have measured in a solvent mixture consisting mainly of protonated species, the scattering intensity of the solvent background is almost identical to that of the micellar solution and, therefore, corrections could not be performed with higher accuracy in the asymptotic range.

For the calculation of the shell the adjustable parameters were $\Delta\rho^2$, R_o, and σ_o. R_c was taken as determined by the core fit. From Figures 5−7 it can be seen that large discrepancies appear in the high Q range. In the asymptotic regime where $Q > \xi(R_G)^{-1}$, the length scales are smaller than the blobs and the scattering is dominated by fluctuations from inside the blobs. In this Q range the scattering is determined by correlations of the excluded volume type, which implies a $Q^{-1/\nu}$ dependence of $d\Sigma(Q)/d\Omega$. Since it is not considered in the theoretical expression, the fitting procedure was carried out only in the low Q range, i.e. 0.004 Å$^{-1} \leq Q \leq$ 0.04 Å^{-1}. Parameters obtained by the fit are also listed in Table 3.

3.2. LALLS Measurements. The weight average molecular weights of the micelles M_W(M) formed in *n*-decane were measured by LALLS. A typical plot is shown in Figure 13. The solutions of the SH 80−10 were bluish and slightly turbid, which indicates the large dimensions of the particles. In this case it was not possible to measure the M_W(M), even at concentrations lower than 1×10^{-6} g/mL, due to the strong scattering. The obtained apparent molecular weights are shown in Table 4. This table also gives the apparent aggregation number $p_W = M_W(M)/M_W(SH)$, where M_W(SH) is the corresponding weight average molecular weight of the super-H-shaped copolymers measured in THF. In case the core consists only of PS-d_8 chains, it is possible to calculate the radii of the cores by using the following equation:

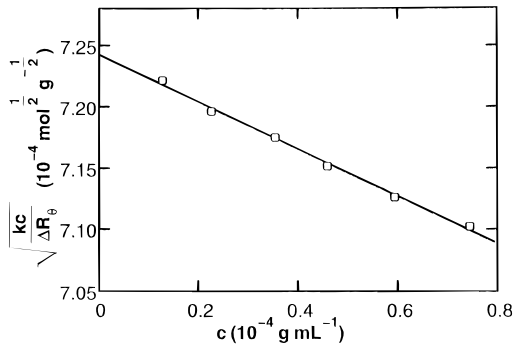

Figure 13. LALLS square-root plot for copolymer SH 40−10 in *n*-decane at 25 °C.

Table 4. LALLS Results for the Aggregated SH Block Copolymers in *n*-Decane

sample	M_W(SH) $\times 10^{-4}$	M_W(M) $\times 10^{-6}$	p_W	amt of PS-d_8 (v %)	R_c[b] (Å)	$A_2 \times 10^4$ (mL mol g^{-2})
SH 40−20	14.9	2.04	14	29	61	−3.6
SH 40−10	11.4	1.91	17	37	65	−1.4
SH 80−10	15.5	(11.4)[a]	(72)[a]	52		

[a] Calculated from eq 11, using the radius obtained by SANS. [b] Calculated from eq 11, using $M_W(M) = p_W M_W(SH)$.

$$R_c = \left(\frac{3p_W x M_W(SH)}{4\pi\rho N_L}\right)^{1/3} \tag{11}$$

where x is the weight fraction of PS-d_8 of the SH copolymer, $\rho = 1.12$ is the density of PS-d_8, and N_L is the Avogadro number. The results (see Table 4) are consistent with the fitted core radii of the SANS experiment.

3.3. Viscosity Measurements. The intrinsic viscosities of the six SH copolymers in *n*-decane at 25 °C were calculated by using the well-known Huggins and Kraemer equations:

$$\frac{\eta_{sp}}{c} = [\eta] + K_H[\eta]^2 c \tag{12}$$

$$\frac{\ln \eta_{sp}}{c} = [\eta] + K_K[\eta]^2 c \tag{13}$$

A typical plot of η_{sp}/c and $(\ln \eta_r)/c$ as a function of c are shown in Figure 14.

The viscometric radii were calculated by using the following equation:

$$R_V = \left(\frac{3[\eta]M_W(M)}{10N_L\pi}\right)^{1/3} \tag{14}$$

The obtained intrinsic viscosities are given in Table 5. In the same table the Huggins constants are listed, together with the calculated viscometric radii of the corresponding SH.

4. Discussion

4.1. Molecular Parameters and Form Factors. The good agreement between the total molecular weight

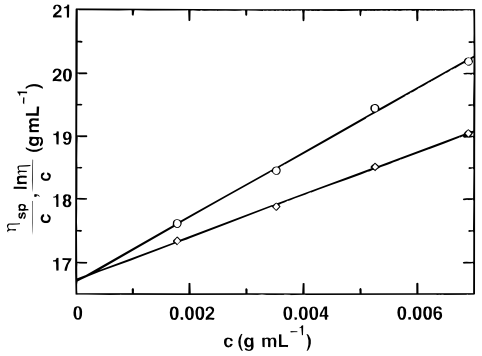

Figure 14. Huggins and Kraemer plots for copolymer SH 40−10.

Table 5. Results from Viscosity Measurements for PS/PI SH Block Copolymers in *n*-Decane

sample	M_W(M) $\times 10^{-5}$	$[\eta]$ (mL g^{-1})	K_H	R_V (Å)	R_G (Å)	R_V/R_G
SH 10−20	1.09[a]	36.1	0.88	85.5	102	0.83
SH 10−10	0.71[a]	32.3	1.1	71.4	86	0.80
SH 20−20	1.28[a]	34.9	0.93	89.2	108	0.81
SH 40−20	20.4	23.4	1.6	192	139[b]	1.37
SH 40−10	19.1	16.7	1.8	172	131[b]	1.31
SH 80−10	114	10.6	1.9	262	190[b]	1.38

[a] The values of the LALLS measurements were used, since no aggregation was found by SANS. [b] Calculated from R_o using eq 17.

of the PI chains of the SH copolymers 20−10, 10−10, and 10−20, found by SANS in the selective solvent and MO obtained in a common good solvent reveals that no aggregation appears. On the contrary the SANS results for SH copolymers 80−10, 40−10, and 40−20 clearly show the formation of aggregates.

From Figures 10−12 it can be seen that the calculated scattering cross section of a homogeneous density hard sphere fits well to the experimental data in the measured Q range. For SH copolymer 80−10 the edge of the core was found to be very shape (smearing parameter σ_c = 5 Å). This can also be taken as a good indication for a low polydispersity by taking into account the large core radius of 130 Å, although $p_W \propto R^3$. For copolymers SH 40−10 and 40−20 the secondary maximum is weak and appears at higher Q values due to the lower core radii. In this Q range the fits are not very sensitive to smearing effects. Therefore, σ_c could not be determined accurately and no statement can be made on the polydispersity of these micelles.

The fitted contrast factors $\Delta\rho^2$ (see Table 3) of the PS-d_8 cores are about 10% lower than those calculated by eq 2. These deviations may be due to small errors caused by the corrections and absolute normalization procedures. They could however be attributed to the existence of a small amount (smaller than 4%) of solvent in the core.

For the PI coronas a hollow sphere model with a constant density profile was used to calculate the theoretical scattering cross sections. A sharp density cutoff of the core-shell interface was assumed. Although this model is very simple, a good agreement between the theoretical and experimental curves was obtained. The fitting procedure was applied in the low Q range only due to the scattering from inside the blobs at high Q, as can be seen from Figures 5−7. The good agreement may be related to the low molecular weights of the arms and the high number of PI chains which appear to fill more or less uniformly the micellar corona. By the fits an average $\Delta\rho$ of 1.22 × 10^{10} cm^{-2} was

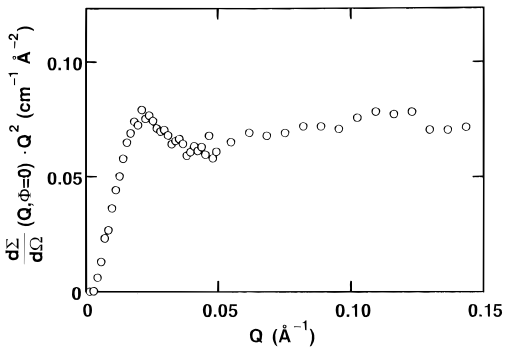

Figure 15. Scattering cross section $d\Sigma(Q,\phi\rightarrow 0)/d\Omega$ of copolymer SH 10−10 in a Kratky representation.

obtained. This value corresponds to a shell with 20% polymeric chains and 80% solvent. In the high Q range the scattering law is $d\Sigma(Q)/d\Omega \propto Q^{-1/\nu}$ where ν is the Flory exponent. The value of ν is equal to $^3/_5$ in the case of excluded volume interactions and 0.5 in the case of Θ conditions. We found increased values of the Flory exponent (ν = 0.62−0.68, see Table 3) by power law fits in the asymptotic high Q range. In the case of regular stars with high functionalities this was attributed to the stretching of the arms.[34,35] It should be noted that the PI arms can be already slightly stretched even without aggregation due to the three-arm star-shaped branch points of the SH structure. Astonishingly, the fitted smearing, σ_0, of the overall radius of the micelle formed by SH copolymer 80−10 is only 5 Å. With respect to the large size (R_0 = 245 Å) it becomes obvious that nearly monodisperse aggregates (see core smearing), which exhibit a sharp density cutoff at the outer periphery, are built by this block copolymer. The corresponding smearing values of copolymers SH 40−10 and SH 40−20 were determined to be 12 and 16 Å, respectively. These slightly increased numbers are mainly attributed to the fuzziness of the outer periphery. Additionally, different processes, e.g. dynamic form fluctuations or small static deviations from the spherelike shape, can contribute to a relatively high smearing in the radius. However, we assume also in these two cases nearly monodisperse aggregates.

By the model fitting, the core radius R_c and the overall radius R_o of the aggregates were determined. The difference between both radii $H = R_o - R_c$ yields information about the thickness of the PI corona. The thickness obtained for copolymers SH 40−20 and SH 40−10 are 116 and 101 Å, respectively. The difference is mainly due to the higher molecular weight of the PI part in SH copolymer 40−20, since the aggregation numbers are similar. For copolymer SH 80−10 we found a shell thickness of H = 115 Å. This is larger than that of copolymer SH 40−10, although the PI chains are identical in both copolymers. We explain this deviation by the higher aggregation number of SH 80−10. Consequently, the PI chains are more closely packed, leading to a stronger radial chain elongation.

As an example for the nonaggregating polymers Figure 15 presents the scattering data of copolymers SH 10−10 under the shell contrast condition in a Kratky representation. In this plot a shallow peak occurs at low Q. A peak in a Kratky representation is a characteristic feature of star form factors[28] and does not appear for linear polymers. From the peak position, Q_{max}, it is possible to determine the radii of gyration by approximating the experimental coherent scattering cross sections by the Gaussian star cross sections, evaluated

by Benoit:[20]

$$\frac{d\Sigma}{d\Omega} = \frac{\Delta\rho^2}{N_L}\phi V_W \frac{2}{fz^4}\left(z^2 - [1 - \exp(-z^2)] + \frac{f-1}{2}[1 - \exp(-z^2)]^2\right) \quad (15)$$

with $z = \sqrt{f/(3f-2)}QR_G$. The peak position determined by $\partial(z^2(d\Sigma/d\Omega))/\partial z = 0$ reveals for a six-arm star

$$z_{max} = 1.37 = 0.61Q_{max}R_G \quad (16)$$

Using the experimental Q_{max}, radii of gyration could be determined. Recently, it was shown that radii of gyration of regular star polymers in a good solvent can be determined accurately by this method.[34] Here, R_G values obtained for copolymers SH 10−20, SH 10−10, and SH 20−20 are about 10% higher than those obtained by Berry plots (see Table 2). However, R_G values of corresponding symmetric PI stars in cyclohexane[27] are in good agreement with R_G (Berry) − R_c (R_c = 18, 15, and 19 Å for SH copolymers 10−20, 10−10, and 20−20; calculated by eq 11). This result implies that the nonaggregating PS/PI super-H block copolymers adopt a starlike profile with a core consisting of the PS-d_8 chain (see Scheme 1).

Another general feature of a Kratky representation is a plateau in the intermediate Q range that appears for polymers in the melt or under Θ conditions ($\nu = 0.5$). By power law fits between $Q = 0.06$ and 0.15 Å^{-1} we obtained ν values approximately equal to 0.55 (see Table 2). This result may indicate that decane is only a marginally good solvent for polyisoprene. This finding is supported by the low second virial coefficient (A_2 = (4−5) × 10^{-4} mL mol g^{-2}) obtained from the SANS data under shell contrast by Berry plots. A regular PI eight-arm star of similar molecular weight shows an A_2 value of about 8 × 10^{-4} mL mol g^{-2} [29] in the good solvent cyclohexane. Furthermore, our results are confirmed by results of Roovers[30] found for polybutadiene in *n*-decane which can be regarded as a similar system.

The apparent molecular weight of the micelles obtained with LALLS in *n*-decane reveals that aggregation exists in concentrations as low as 2 × 10^{-5} g/mL (see Figure 13). As a consequence, the cmc of these copolymers appears in very low concentrations. A similar result was found for high molecular weight diblock copolymers in a selective solvent for PI.[5]

The molecular weight of aggregates of the SH can be calculated from the core radius obtained by SANS and their composition (eq 11), assuming there is no solvent in the PS-d_8 core. The molecular weights calculated for the SH polymers 40−10 and 40−20 is 2.1 × 10^6 and 2.35 × 10^6 g/mL, respectively. They are slightly larger than those found by LALLS. It should be noted that the LALLS experiments were performed in concentrations which were 2 orders of magnitude lower than those of the SANS experiments. Therefore, in the concentration range of the LALLS measurements, which is closer to the cmc, the aggregation number could be slightly smaller. However, the deviation is small and within the experimental error of the two methods, in particular, when we compare the corresponding core radii.

The relatively high intrinsic viscosities of the copolymers SH 10−10, 10−20, and 20−20, compared to those of the copolymers SH 80−10, 40−10, and 40−20 in the same solvent, is another indication that the latter copolymers are aggregated, while the former do not form polymolecular micelles. The viscometric radius, R_V, is related to [η] and the molecular weight of the micelle, M_W(M), by eq 14. When the polymeric chains aggregate, the molecular weight increases, while the radius does not increase significantly. Therefore, the intrinsic viscosity has to decrease, especially when the aggregation number is very high. This can be seen from the low value of [η] = 10.6 mL/g of the SH 80−10 block copolymer. Comparing the intrinsic viscosity of the high molecular weight sample SH 80−10 with that one of the low molecular weight sample SH 10−10 ([η] = 32.4 mL/g) reveals a considerable increase.

The R_G values of the overall spherical micelles can be calculated by the following equation:

$$R_G^2 = \frac{3}{5}R_o^2 \quad (17)$$

The calculated R_G values are shown in Table 5. The ratio $R_V/R_G \simeq 0.81$ of the nonaggregated copolymers lies between the corresponding ratio experimentally found for linear PI homopolymers (≃0.8) and those of the symmetric six-arm PI stars in a good solvent (≃0.9).[27] The latter ratio of the aggregated SH was found to be between 1.3 and 1.4 (see Table 5). These values are close to those found by Roovers et al.[31] for regular stars with high functionalities and implies a hard-sphere behavior of the micelles.

Table 6. Molecular Characteristics of the Micelles of Linear PS/PI Diblock Copolymers

sample	N_S	N_I	R_H (Å)	R_c[a] (Å)	H[e] (Å)	solvent	p_W
SI1[b]	154	294	275	119	156	*n*-heptane	278
SI2[b]	183	294	300	141	159	*n*-heptane	386
SI3[b]	279	294	380	194	186	*n*-heptane	666
SI4[b]	317	294	460	240	220	*n*-heptane	1113
SI5[d]	125	559		56		*n*-decane	36
SB1[c]	271	1015	500	102		*n*-decane	100

[a] Calculated from eq 11. [b] From ref 6. [c] From ref 32. [d] From ref 36. [e] Calculated by $H = R_H - R_C$.

Table 7. Molecular Characteristics of the Micelles of PS/PI SH Block Copolymers in *n*-Decane

sample	N_S	N_I	R_V (Å)	R_c (Å)	H[a] (Å)	p_W
SH 10−20	75	1376				1
SH 10−10	75	802				1
SH 20−20	150	1580				1
SH 40−20	410	1376	192	63	129	14
SH 40−10	410	802	172	69	103	17
SH 80−10	755	802	262	130	132	72

[a] Calculated by $H = R_V - R_c$.

4.2. Influence of the Architecture. In general, the capability of block copolymers to form micelles in a selective solvent is mainly determined by the composition of the copolymers. Thereby, the aggregation number increases with increasing fraction of the insoluble block. Furthermore, the aggregation behavior is dependent on the total molecular weight of the block copolymer. There exist certain limits respecting composition and molecular weight beyond which the block copolymers are insoluble.[5]

In order to discuss the influence of the architecture on these properties we will now compare the results of the super-H-shaped block copolymers with those of linear PS/PI diblocks obtained from the literature. Tables 6 and 7 present the molecular and micellar characteristics of linear PS/PI block copolymers and of PS/PI SH block copolymers, respectively. In four cases heptane was used as a selective solvent for the linear copolymers, but since the quality of both solvents is comparable a qualitative discussion is possible. The aggregation number p_W as a function of the composition for both architectures has been plotted in Figure 16. It

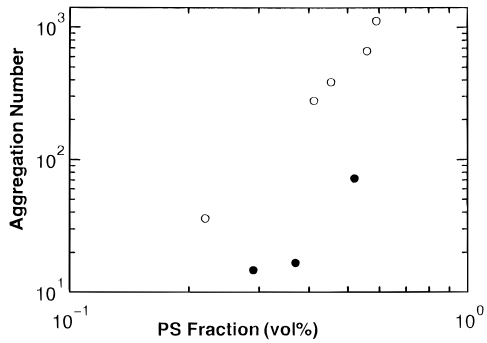

Figure 16. Aggregation number as a function of the volume fraction of PS for linear diblocks (○) and for the SH copolymers (●).

Scheme 2

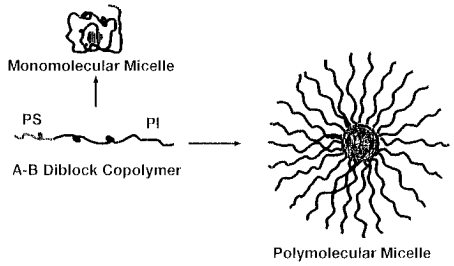

can be seen that p_W increases steeply with increasing PS fraction in both cases. The interesting feature is that the aggregation numbers of the SH copolymers are almost 1 order of magnitude lower than those of the corresponding linear diblocks. However, due to the six branches in each SH the total number of arms of the micelles are comparable. For example, if we compare the micelles of the SH 80−10 and SI 3 (see Tables 6 and 7) which are copolymers with similar compositions, the number of PI chains are 432 and 666, respectively, although the aggregation number of the SH polymer is only 72.

It was reported by Oranli et al.[5] that a PS/PB block copolymer that contains approximately 52% PS and has a total molecular weight of 7.2×10^4 is not soluble by heating in *n*-alkanes at 60 °C. In the case of SH copolymer 80−10 the amount of PS-d_8 is 58 w % and the molecular weight 8.54×10^4. Apparently, the SH architecture improves the solubility properties compared to linear diblocks, due to the higher number of PI arms.

On the other hand the SH 20−20 with a PS-d_8 fraction of 13.5% did not aggregate under the experimental conditions. From experimental data of a PS/PB system it is known that polymolecular micelles are formed from block copolymers containing 15 w % PS.[13] This difference can be visualized in Schemes 1 and 2. A monomolecular micelle formed by the SH copolymers presents similarities with a polymolecular micelle of aggregation number 6 of a linear diblock copolymer. The relatively small PS core is well protected by the six PI arms of the SH structure. Thus it becomes obvious that the tendency to aggregate is strongly reduced.

4.3. Interpretation in Terms of Scaling Models. The architecture of super-H block copolymers (A_3BA_3) modifies the aggregation behavior in a selective solvent for the A blocks compared to that of AB diblock copolymers. Two effects are involved. The first concernes the configuration of the isolated, nonaggregated SH_s. In a selective solvent it consists of a collapsed B core surrounded by a swollen corona of A blocks. It is thus reminiscent of a starlike micelle rather than of the tadpole-like configurations attributed to AB diblock copolymers. As we shall see, this feature affects the chemical potential of the isolated SH_s. It may also contribute to the solubilization of the SH_s via enhanced colloidal stabilization due to the corona; i.e., the coronal repulsion may prevent precipitation. Second, micelles of SH_s tend to have denser coronas as compared to micelles, with the same aggregation number, formed by AB diblock copolymers. This is because each aggregated SH contributes a number of arms to the corona while each AB diblock contributes only a single coronal chain. This second feature increases the coronal penalty, thus favoring smaller aggregation numbers.

To quantify these remarks, we consider an SH block copolymer consisting of a central B block comprising N_B monomers. Each of its end groups supports an A star polymer consisting of $f/2$ arms, each comprising N_A monomers. For simplicity the size of all monomers is assumed to be equal, a. We focus, for brevity, on the case $f \gg 1$. We further limit the discussion to two out of three main micellar structural regimes. First we treat the limit of starlike micelles[1,38] where the thickness of the corona, H, is much larger than the radius of the core, $H \gg R_c$. In this case the overall micellar size, R_o, is mostly due to the corona, $R_o \approx H$. The coronal structure of such micelles is essentially that of star polymers.[1,39] For SH micelles, the requirement $H \gg R_c$ is satisfied when $N_B \ll N_A^{15/11} f^{2/5}$ as compared to $N_B \ll N_A^{15/11}$ for the case of AB diblocks.

In the second, intermediate,[40] regime $H \leq R_c$ the coronal free energy penalty, F_{corona}, is dominant in comparison to the stretching penalty of the p core blocks, $F_{core}/kT \approx pR_c^2/N_B a^2$. While $F_{corona} \gg F_{core}$ for both regimes, in the second case F_{corona} assumes a different form since the coronal structure is essentially that of a flat polymer brush[1,41] rather than that of a star polymer. For SH micelles the intermediate regime occurs when $N_A^{15/11} f^{2/5} \ll N_B \ll N_A^{18/11} f^{7/6}$ as compared to $N_A^{15/11} \ll N_B \ll N_A^{18/11}$ in the diblock case. Note that the intermediate regime is larger for SH micelles. The third structural regime, of crewcut micelles[42] for which $H \ll R_c$ and $F_{corona} \ll F_{core}$, is not considered since such micelles are expected to be less stable than the corresponding lamellae.[40]

Finally, we confine the analysis to SH_S for which the intrachain micelles formed by single polymers are starlike; i.e., the coronal radius $f^{1/5} N_A^{3/5} a$ is much larger than the core radius $N_B^{1/3} a$ or $N_B \ll N_A^{9/5} f^{3/5}$. Accordingly, the chemical potential of the nonaggregated chains may be written as

$$\mu/kT \approx \ln \phi + f^{3/2} + (\gamma a^2/kT) N_B^{2/3} \qquad (18)$$

The first term allows for the translational entropy of free chains whose volume fraction is ϕ. The second term allows for repulsive monomer−monomer interactions within the starlike corona, and the third term reflects the surface free energy of the core, whose surface tension is γ. Note that the second term is distinctive to the SH polymers and is absent in AB diblock copolymers. The other two terms appear in both systems. The free energy of a starlike micelle comprised of p chains is

$$F_{micelle}/kT \approx p^{3/2} f^{3/2} + p^{2/3} N_B^{2/3} (\gamma a^2/kT) \qquad (19)$$

Repulsive monomer−monomer interactions within the starlike corona are described by the first term. The second term allows for the surface free energy of the core $F_{interface} \approx \gamma R_c^2$ where $R_c \approx p^{1/3} N_B^{1/3} a$. Note that in starlike micelles of AB diblocks there is no $f^{3/2}$

dependence since $f = 1$. With this important caveat, this expression is identical to that found for starlike micelles formed by AB diblock copolymers.

To obtain the equilibrium aggregation number, p_{eq}, as well as the critical micelle concentration, ϕ_{cmc}, and the chemical potential at the cmc, μ_{cmc}, it is convenient to use the grand canonical picture introduced by Marques et al.[43] The relevant grand canonical potential is

$$\Omega/kT \approx F_{micelle}/kT - p\mu/kT \quad (20)$$

The above quantities are determined by two conditions: $\Omega = 0$ and $\partial\Omega/\partial p = 0$. For starlike micelles these two conditions lead to

$$p_{eq} \approx N_B^{4/5} f^{-9/5} (\gamma a^2/kT)^{6/5} \quad (21)$$

This is significantly smaller than $p_{eq} \approx N_B^{4/5}(\gamma a^2/kT)^{6/5}$ obtained in the case of starlike micelles of AB diblock copolymers. The span of the SH starlike micelle is accordingly $R_o/a \approx N_B^{4/25} f^{-9/25} N_A^{3/5} (\gamma a^2/kT)^{6/25}$ while $R_c/a \approx f^{-3/5} N_B^{3/5} (\gamma a^2/kT)^{6/5}$. These values are smaller by factors of $f^{-9/25}$ and $f^{-3/5}$ than the corresponding radii of starlike diblock micelles. Upon substitution of eq 21 in the expression for μ as obtained from $\partial\Omega/\partial p = 0$ one obtains

$$\mu_{cmc}/kT \approx f^{6/10} N_B^{2/5} (\gamma a^2/kT)^{3/5} \quad (22)$$

This value is larger by a factor of $f^{6/10}$ than the μ_{cmc} of AB diblocks. Finally, by comparing this μ_{cmc} to the μ as given by eq 18 we obtain

$$\phi_{cmc} \approx \exp[(\gamma a^2/kT) f^{3/5} N_B^{2/5} (1 - N_B^{4/15}/f^{3/5}) - f^{3/2}] \quad (23)$$

In the intermediate regime F_{corona} assumes a different form, corresponding to a flat polymer brush.[1] The free energy per coronal chain is thus $kTN_A(a^2/\sigma)^{5/6}$ where $\sigma \approx R_c^2/p$ is the area per chain. Accordingly, $F_{corona}/kT \approx pPN_A(a^2/\sigma)^{5/6} \approx f^{11/6} p^{23/18} N_B^{-5/9} N_A$. The interfacial term remains unmodified, thus leading to

$$F_{micelle}/kT \approx f^{11/6} p^{23/18} N_B^{-5/9} N_A + p^{2/3} N_B^{2/3} (\gamma a^2/kT) \quad (24)$$

Following the procedure outlined above, we obtain

$$p_{eq} \approx f^{-3} N_B^2 N_A^{-18/11} (\gamma a^2/kT)^{18/11} \quad (25)$$

as compared with $p_{eq} \approx N_B^2 N_A^{-18/11} (\gamma a^2/kT)^{18/11}$ for diblock micelles. This leads to $R_c/a \approx f^{-1} N_B N_A^{-6/11} (\gamma a^2/kT)^{6/11}$ and to $H/a \approx f^{-1/3} N_A^{9/11} (\gamma a^2/kT)^{2/11}$. These are smaller by factors of f^{-1} and $f^{-1/3}$ than the corresponding values for micelles formed by diblock copolymers. Finally μ_{cmc} in this regime is

$$\mu_{cmc}/kT \approx f^{-5/6} N_A^{6/11} (\gamma a^2/kT)^{6/11} \quad (26)$$

This is smaller by a factor of $f^{-5/6}$ than the μ_{cmc} of diblock micelles in the intermediate regime.

Now we test the above derived scaling laws by the experimental results of the super-H and the linear PS/PI block copolymers. In Tables 6 and 7 the core and shell dimensions are listed. It can be seen that $R_c \leq H$ for all micelles. Therefore, it appears to be difficult to decide whether the starlike or the intermediate regime is appropriate to describe the micellar behavior. By using the conditions $N_S \ll N_I^{15/11} f^{2/5}$ and $N_I^{15/11} f^{2/5} \ll N_S$ $\ll N_I^{18/11} f^{7/6}$ (N_S and N_I are the numbers of styrene and isoprene monomers, and f is the functionality of the unaggregated block copolymers which is 1 for the linear and 6 for the super-H structure), the experimental molecular weights would indicate the starlike regime. However, it may be that a constant factor shifts the calculated numbers from the starlike to the intermediate regime. In order to distinguish between the two regimes we have plotted the aggregation number, p_W, as a function of $N_S^{4/5} f^{-9/5}$ and $N_S^2 N_I^{-18/11} f^{-3}$ according to eqs 21 and 25. In the case of a validity of the corresponding equations straight lines are expected. The plots are shown in Figures 17 and 18. It can be seen that the scaling law for the starlike model does not represent the experimental data. In this plot the aggregation numbers do not even follow a systematic dependence on the scaling variable. On the other hand the scaling relation for the intermediate regime fairly well describes the aggregation behavior of the PS/PI block copolymers. The dependence of the core radius, R_c, on N_I, N_S, and f according to the prediction in the intermediate regime is shown in Figure 19. The values of both linear and SH structure are well represented by this scaling law. In contrast the corresponding power

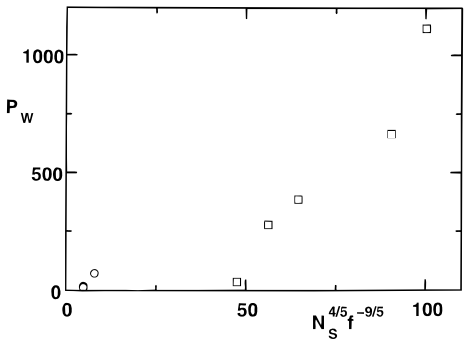

Figure 17. Aggregation number plotted according to the scaling law in the starlike regime (eq 21): linear (□); SH (○).

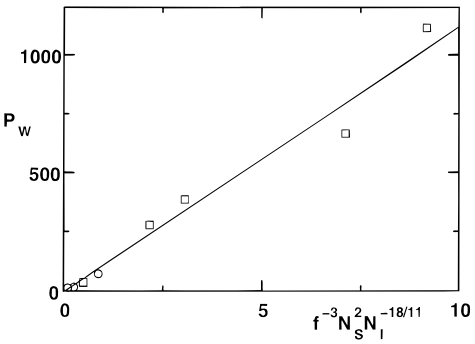

Figure 18. Aggregation number plotted according to the scaling law in the intermediate regime (eq 25): linear (□); SH (○).

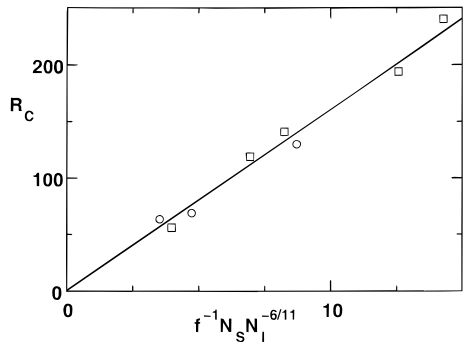

Figure 19. Core radii plotted according to the scaling law in the intermediate regime: linear (□); SH (○).

law dependence of the shell thickness, H, does not show the expected behavior: A constant number of segments, N_I, should lead to a constant thickness of the corona for both architectures. It should be mentioned that H was calculated by $R_{V,H} - R_c$ assuming that R_V and R_H are equal. Measurements on multiarm star polymers revealed that R_H and R_V are identical within experimental error.[31] Furthermore, it appears to be justified to combine dynamic and static radii since the spherelike character of the micelles was shown by our SANS results. In the case of monodisperse spheres $R_{V,H} = R_o = R_c + H$. Although small deviations were found between R_V and R_o (Tables 3 and 5)—indicating experimental uncertainty—the corona grows considerably with constant number of monomers, N_I. This can be clearly seen in the case of the linear block copolymers, where H increases from 156 to 220 Å, while $N_I = 294$ in all cases. Thus, while the experimental results show some encouraging agreement with predictions of the scaling model, there still appear to be problems with a correct description of the corona. Further, more systematic investigations concerning molecular weight, composition, and architecture of the block copolymers will be needed to finally scrutinize the theoretical picture.

5. Conclusions

In this paper we have presented a study of the micellar properties of model super-H-shaped PS/PI block copolymers. The polymers were prepared by anionic polymerization techniques using tetrachlorosilane as the linking agent. The polymers were thoroughly characterized by MO, VPO, SEC−UV, and LALLS. The results obtained reveal a high degree of chemical and molecular homogeneity.

The micellar behavior of these block copolymers was investigated in *n*-decane which is a selective solvent for the PI part. A combined examination by SANS, LALLS, and viscometry was performed in order to determine the micellar characteristics. The experimental results can be summarized as follows: (i) Super-H block copolymers with a large fraction (≥33%) of polystyrene aggregate to near monodisperse, spherical micelles. Those with a small PS content (≤14%) are nonaggregated under the experimental conditions. (ii) In comparison with linear PS/PI diblock copolymers the solubility is increased and the aggregation number is almost 1 order of magnitude smaller.

The scaling models of the intermediate and starlike micellar structure were extended to allow for the number of arms. The derived scaling laws were proofed by the experimental results of the SH and linear block copolymers. Thereby, the dependence of the aggregation number, p_W, on the functionality, f, and on the number of isoprene, N_I, and styrene segments, N_S, follows the predicted behavior of the intermediate model. Also, the radius of the core, R_c, as a function of f, N_S, and N_I is well represented by the intermediate model. The corona thickness, however, does not show the expected behavior.

Acknowledgment. We would like to thank the Laboratoire Léon Brillouin for providing us the SANS beam time. We are also grateful to Dr. J. Roovers for making many helpful remarks and Mr. Dieter Schneiders for providing us the programs for the calculation of the theoretical curves.

References and Notes

(1) Halperin, A.; Tirrell, M.; Lodge, T. P. *Adv. Polym. Sci.* **1992**, *100*, 31.
(2) Gast, A. P. *Scientific Methods for the Study of Polymer Colloids and Their Applications*; Kluwer Academic Publishers: Dordrecht, The Netherlands, 1990; pp 311−328.
(3) Tuzar, Z.; Kratochvil, P. *Advances in Colloid and Interface Science*; Elsevier: Amsterdam, 1976.
(4) For the present paper we will use the term micelle for block copolymers in a selective solvent in which the soluble part keeps the insoluble in solution, independent of aggregation occurring or not.
(5) Oranli, L.; Bahadur, P.; Riess, G. *Can. J. Chem.* **1985**, *63*, 2691.
(6) Bahadur, P.; Sastry, N. V.; Marti, S.; Riess, G. *Colloids Surf.* **1985**, *16*, 337.
(7) Gallot, Y.; Franta, P.; Rempp, P.; Benoit, H. *J. Polym. Sci., Part C* **1964**, *4*, 473.
(8) Kotaka, T.; Tanaka, T.; Hattori, M.; Inagaki, H. *Macromolecules* **1978**, *11*, 138.
(9) Periard, J.; Riess, G. *Eur. Polym. J.* **1973**, *9*, 687.
(10) Selb, J.; Gallot, Y. *Makromol. Chem.* **1980**, *182*, 1491.
(11) Higgins, J. S.; Dawkins, J. V.; Maghami, G. G.; Shakir, S. A. *Polymer* **1986**, *27*, 931.
(12) Plestil, J.; Baldrian, J. *Makromol. Chem.* **1975**, *176*, 1009.
(13) Bluhm, T. L.; Malhorta, S. L.; Hong, M.; Noolandi, J. *Polym. Prepr. (Am. Chem. Soc., Div. Polym. Chem.)* **1983**, *24*, 405.
(14) Hadjichristidis, N.; Iatrou, H.; Behal, S. K.; Chludzinski, S. J.; Disko, M. M.; Garrer, T. R.; Liang, K.; Lohse, J. D.; Milner, S. T. *Macromolecules* **1993**, *26*, 5812.
(15) Morton, M.; Fetters, L. J. *Rubber Chem. Technol.* **1975**, *48*, 359.
(16) Roovers, J.; Toporowski, P. *Macromolecules* **1983**, *16*, 843.
(17) Iatrou, H.; Hadjichristidis, N. *Macromolecules* **1992**, *25*, 4649.
(18) Iatrou, H.; Hadjichristidis, N. *Macromolecules* **1993**, *26*, 2479.
(19) Duval, M.; Duplessix, R.; Picot, C.; Rempp, P.; Benoit, H.; Cotton, J. P.; Farnoux, B.; Ober, R. *J. Polym. Sci., Part B* **1976**, *14*, 585.
(20) Benoit, H. *J. Polym. Sci.* **1953**, *11*, 507.
(21) Ionescu, L.; Duval, M.; Duplessix, R.; Picot, C.; Benoit, H. *J. Polym. Sci., Polym. Phys. Ed.* **1981**, *19*, 1019.
(22) Gurevich, I. I.; Tarasov, L. V. *Low Energy Neutron Physics*; North-Holland: Amsterdam, 1968.
(23) Bacon, G. E. *Acta Crystallogr.* **1972**, *A28*, 357.
(24) Iatrou, H.; Avgeropoulos, A.; Hadjichristidis, N. *Macromolecules* **1994**, *27*, 6232.
(25) Roovers, J.; Toporowski, P. *Macromolecules* **1981**, *14*, 1174.
(26) Pedersen, J. S.; Posselt, D.; Mortensen, K. *J. Appl. Crystallogr.* **1990**, *23*, 321.
(27) Bauer, J. B.; Fetters, L. J.; Graessley, W. W.; Hadjichristidis, N.; Quack, F. G. *Macromolecules* **1989**, *22*, 2337.
(28) Burchard, W. *Macromolecules* **1977**, *10*, 919.
(29) Willner, L.; Jucknischke, O.; Richter, D.; Farago, B.; Fetters, L. J.; Huang, J. *Europhys. Lett.* **1992**, *19* (4), 297.
(30) Roovers, J. Private communication.
(31) Roovers, J.; Zhou, L. L.; Toporowski, P. M.; Van der Zwan, M.; Iatrou, H.; Hadjichristidis, N. *Macromolecules* **1993**, *26*, 4324.
(32) Tsunashima, Y.; Hirata, M.; Kawamata, Y. *Macromolecules* **1990**, *23*, 1089.
(33) Berry, G. C. *J. Chem. Phys.* **1966**, *44*, 4350.
(34) Willner, L.; Jucknischke, O.; Richter, D.; Roovers, J.; Zhou, L.-L.; Toporowski, P.; Fetters, L. J.; Huang, J.; Lin, M.; Hadjichristidis, N. *Macromolecules* **1994**, *27*, 3821.
(35) Grest, G. S.; Kremer, K.; Witten, T. A. *Macromolecules* **1987**, *20*, 1376.
(36) Price, C.; McAdam, J. G.; Lally, T. P.; Woods, D. *Polymer* **1974**, *15*, 228.
(37) Xu, R.; Winnik, M. A.; Riess, G.; Chu, B.; Croucher, M. D. *Macromolecules* **1992**, *25*, 644.
(38) Halperin, A. *Macromolecules* **1987**, *20*, 2943.
(39) Daoud, M.; Cotton, J. P. *J. Phys.* **1982**, *43*, 531.
(40) Izzo, D.; Marques, C. M. *Macromolecules* **1993**, *26*, 7194.
(41) Alexander, S. *J. Phys.* **1977**, *38*, 983.
(42) de Gennes, P. G. In *Solid State Physics*; Liebert, L., Ed.; Academic Press: New York, 1978; Suppl. 14.
(43) Marques, C.; Joanny, J. F.; Leibler, L. *Macromolecules* **1988**, *21*, 1051.

MA9509063